PUBLICATION V

Temperature majorant cross sections in Monte Carlo neutron tracking

Nucl. Sci. Eng., Accepted for publication Aug 31, 2014.

Temperature Majorant Cross Sections in Monte Carlo Neutron Tracking

Revised version: March 31, 2015

(Mr.) Tuomas Viitanen and (Dr.) Jaakko Leppänen

VTT Technical Research Centre of Finland

tuomas.viitanen@vtt.fi, jaakko.leppanen@vtt.fi

Send Correspondence to:

Tuomas Viitanen

VTT Technical Research Centre of Finland

P. O. Box 1000, FI-02044 VTT, Finland

Email: tuomas.viitanen@vtt.fi

Telephone: +358 40 763 1963

No. of pages: 35

No. of tables: 3

No. of figures: 8

Temperature Majorant Cross Sections in Monte Carlo Neutron Tracking

Tuomas Viitanen and Jaakko Leppänen

Abstract

This article discusses the generation of temperature majorant cross sections, the type of cross sections required by two separate techniques related to Monte Carlo neutron tracking, namely the Doppler-broadening rejection correction (DBRC) and Target Motion Sampling (TMS) temperature treatment methods. In the generation of these cross sections the theoretically infinite range of thermal motion must be artificially limited by applying some sort of a cut-off condition, which affects both the accuracy and the performance of the calculations. In this article, a revised approach for limiting the thermal motion is first introduced and, then, optimal cut-off conditions are determined for both the traditional majorant, commonly used in DBRC implementations and old implementations of the TMS method, and the revised majorant.

It turns out that using the revised type of temperature majorant cross sections increases the performance of the TMS method slightly, but no practical difference is observed with the DBRC method. It is also discovered that in ordinary reactor physical calculations the cut-off conditions originally adopted from the SIGMA1 Doppler-broadening code can be significantly relieved without compromising the accuracy of the results. By updating the cut-off conditions in the majorant generation, the CPU time requirement of Serpent 2.1.17 is reduced by 8–23 % in TMS calculations and by 1–6 % in problems involving DBRC.

Keywords: Monte Carlo, DBRC, on-the-fly, Doppler-broadening, temperature majorant cross section

I. Introduction

Thermal motion affects the neutronics of a reactor system in basically two ways. First, the thermal oscillation of nuclei changes the probabilities at which neutrons interact with matter, affecting the reaction rates and mean free paths within the system. Second, thermal motion also has impact on the collision physics of scattering events.

In conventional Monte Carlo neutron transport, the effects on reaction rates are taken into account by using effective, Doppler-broadened cross sections that are prepared before the transport calculation. The effect of thermal motion on scattering is usually modeled during the transport calculation by sampling the target motion from a Maxwellian-based distribution each time an elastic scattering occurs, and solving the kinetics of the event according to the sampled velocity. The same procedures cannot be directly applied for bound nuclides (for instance H in H_2O) in the thermal energy region, so for these nuclides the Doppler-broadening and elastic scattering models have to be completed using additional thermal scattering data consisting of special bound scattering cross sections and so-called $S(\alpha, \beta)$ data for secondary particle distributions [1].

Previously, two separate but loosely related techniques that supplement the conventional way of modeling the thermal motion have been introduced. Doppler-broadening rejection correction (DBRC) method, as described in Ref. [2], accounts for the effect of thermal motion induced variation of scattering cross sections on the secondary particle distributions of elastic scattering events. This effect has been traditionally omitted by assuming energy-independent scattering cross sections, but the effect is known to be important especially in case of heavy nuclides with significant resonances in the epithermal energy region. The Target Motion Sampling (TMS) temperature treatment technique, for its part, is a neutron tracking method for taking the effect of thermal motion on reaction rates into account on-the-fly during a Monte Carlo neutron tracking calculation. On-the-fly temperature treatment techniques in general can be used to reduce the memory consumption of transport problems involving materials at numerous temperatures, for example in multi-physics applications of Monte Carlo. The TMS method has been introduced in English by the authors in Refs. [3, 4], but it was recently learned that a similar method has been previously presented in a Russian journal [5] and has been routinely used, for example, in the Monte Carlo transport code PRIZMA for many years [6].

The TMS and DBRC methods have two features in common. First, both of the methods are based on rejection sampling and, second, the rejection sampling techniques of both

methods require a special type of cross sections, called temperature majorant cross sections in the current article. The generation of these cross sections is otherwise straightforward, but the generation process involves determining of a finite range for the relative velocity between the neutron and the target nucleus, which is physically not bounded by any maximum value. Hence, some kind of approximation must be applied in the generation process and this approximation is open to discussion. Traditionally, the thermal motion has been limited by simply truncating the Maxwellian velocity distribution of the target and using the corresponding maximum and minimum relative velocity to determine the energy range of thermal motion. The cut-off condition commonly used in the current implementations of the DBRC method is 16 $k_{\mathrm{B}}T$, where k_B is the Boltzmann constant and T is the temperature of the target nucleus. This condition has been adopted from the SIGMA1 Doppler-broadening code (Ref. [7]) by the developers of the DBRC method [2], and the same condition has been further also used in the implementation of the TMS method in Monte Carlo reactor physics code Serpent[a] due to historical reasons [3].

It has been shown by Becker et al. that using the SIGMA1 cut-off condition results in the correct scattering kernel [2], but no studies were found on the practicality of this cut-off condition. Since both DBRC and TMS are based on rejection sampling, their performance is strongly dependent on the truncation of the thermal motion. Hence, the cut-off deserves a thorough discussion. The previous results in Ref. [8] and the fact that a less-conservative 9 $k_{\mathrm{B}}T$ cut-off has been successfully used together with the on-the-fly temperature treatment method in PRIZMA give rise to a suspicion that the 16 $k_{\mathrm{B}}T$ cut-off is overly conservative and, thus, leads to a waste of computing resources at least when applied with the TMS method.

A new approach for truncating the thermal motion was previously introduced by the authors in the M&C 2013 conference [8]. This idea is refined in the current article, and the properties of this "revised" majorant are compared to the "traditional" majorants. In addition, suggestions for the cut-off conditions to be used with both of the majorant types are determined by applying the majorants in practical calculations involving TMS and DBRC. Since the field of application for the TMS and DBRC methods is limited to free atoms at thermal and resolved resonance energy regions, bound-atom scattering and the unresolved resonance region are left outside the current article.

An introduction to the temperature majorant cross sections and their applications in Monte Carlo neutron tracking is provided in Section II., and the two methods for limiting the range of thermal motion in the majorant generation are presented in Section III. In

[a]For a complete and up-to-date description, visit Serpent website — http://montecarlo.vtt.fi

Section IV., properties of the majorant types are first studied and, then, optimal values of the corresponding cut-off conditions are determined for reactor applications. Serpent 2 is updated in light of the new results and final performance measures are also provided in the same Section. The last Section V. is left for summary and conclusions.

II. Temperature Majorants in Monte Carlo Neutron Tracking

The temperature majorant Σ_{maj} of a cross section Σ is defined

$$\Sigma_{\mathrm{maj}}(E) = \max_{E' \in [E_{\mathrm{min}}, E_{\mathrm{max}}]} \Sigma(E') \,, \tag{1}$$

where E' represents the relative (or target-at-rest) energies between a neutron with laboratory frame-of-reference (L-frame) energy E and a target nucleus in thermal motion[b]. The energy range of E' is limited by energies E_{min} and E_{max} that define the range of thermal motion.

With DBRC, the cross section Σ in Eq. (1) is always an elastic scattering cross section at zero Kelvin, $\Sigma_{\mathrm{s}}(E', 0\ \mathrm{K})$. With TMS method the majorant is based on the total cross section, which may be either a zero Kelvin cross section or a Doppler-broadened effective cross section at an above-zero temperature. Thus, the majorant cross section depends on both the temperature of the basis cross section, T_{base}, and the temperature difference between the T_{base} and the majorant, ΔT. By including the explicit temperature dependencies in Eq. (1), definition

$$\Sigma_{\mathrm{maj}}(E, \Delta T, T_{\mathrm{base}}) = \max_{E' \in [E_{\mathrm{min}}, E_{\mathrm{max}}]} \Sigma(E', T_{\mathrm{base}}) \,, \tag{2}$$

is obtained. Temperature majorant cross sections are illustrated in Figure 1.

The only open question in the majorant generation is related to the choosing of the energy range of the target-at-rest energies E' in Eq. (2). It is practical to approach this problem via velocities, which can be easily converted to energies using the classical relation between the kinetic energy and the velocity

$$E' = \frac{1}{2} M_{\mathrm{n}} v'^2 \,, \tag{3}$$

where M_n is the neutron mass. The relative velocity of the neutron to the target, also known as the target-at-rest velocity, can be obtained from equation

$$v' = \sqrt{v^2 + V_{\mathrm{t}}^2 - 2 v V_{\mathrm{t}} \mu} \,, \tag{4}$$

[b]To be precise, also each cross section Σ_x for which $\Sigma_x(E) \geq \Sigma_{\mathrm{maj}}(E)$ can be considered a temperature majorant cross section of $\Sigma(E')$, but usually it is practical to choose the majorant according to Eq. (1).

where v is the velocity of the neutron, V_t is the velocity of the target and μ is the cosine between the directions of the neutron and the target motion. The target velocity distribution is traditionally assumed to obey the Maxwell-Boltzmann distribution

$$P_\mathrm{MB}(V_\mathrm{t}, T, A)dV_\mathrm{t} = \frac{4}{\sqrt{\pi}}\gamma(T,A)^3 V_\mathrm{t}^2 e^{-\gamma(T,A)^2 V_\mathrm{t}^2} dV_\mathrm{t}\,, \tag{5}$$

where

$$\gamma(T, A) = \sqrt{\frac{AM_\mathrm{n}}{2k_\mathrm{B}T}}\,, \tag{6}$$

A is the ratio of the nuclide mass to M_n.

It should be noted that the distribution in Eq. (5) has an infinite tail and, consequently, an unambiguous maximum velocity for the target cannot be specified. Hence, to get a finite interval for the target-at-rest velocity v' and the corresponding energy, some kind of approximation is required. Two different ways, namely a traditional and a new, revised way, of limiting the thermal motion are presented in Section III. Before going into details of these approximations, the application of the temperature majorant cross sections with the DBRC and TMS methods is shortly presented in Sections II.A. and II.B., respectively.

II.A. Doppler-broadening Rejection Correction

In Monte Carlo neutron tracking, the kinetics of the elastic scattering events can be solved using a few different approaches. The simplest way to treat elastic scattering from free atoms is to assume that the target nucleus is at rest or, in other words, at zero Kelvin temperature. This approximation corresponds to so-called asymptotic scattering kernel, which omits all up-scattering effects, but acts as a reasonable approximation at relatively high neutron energies.

At lower energies, the thermal motion of the target nuclei must be taken into account to correctly model the slowing-down of neutrons. In the conventional free gas treatment, when an elastic scattering event occurs, the velocity of the target nuclide i is first sampled from distribution [9]

$$P_\mathrm{FGT}(V_\mathrm{t}, \mu, T, A_i)dV_\mathrm{t}d\mu = C\Big\{\frac{v'}{2v}P_\mathrm{MB}(V_\mathrm{t}, T, A_i)\Big\}dV_\mathrm{t}d\mu\,, \tag{7}$$

where C is a constant, and the kinetics are then solved conserving the energy and momentum. This sampling scheme involves the assumption that the scattering cross section of the target nuclide is constant and, thus, the secondary particle distributions correspond to a cross section independent scattering kernel.

More detailed description of the elastic scattering requires that also the energy dependence of the scattering cross section is taken into account. This can be done by inserting an additional rejection in the conventional sampling procedure[c]. With this so-called Doppler-broadening rejection correction the target velocity distribution becomes [2]

$$P_{\mathrm{DBRC}}(V_{\mathrm{t}},\mu,T,A_i)dV_{\mathrm{t}}d\mu = C'\Big\{\frac{\Sigma_{\mathrm{s},i}(v',0)}{\Sigma_{\mathrm{maj,s},i}(v,T,0)}\Big\}\Big\{\frac{v'}{2v}P_{\mathrm{MB}}(V_{\mathrm{t}},T,A_i)\Big\}dV_{\mathrm{t}}d\mu\,, \tag{8}$$

where the cross sections $\Sigma_{\mathrm{s},i}(v',0)$ and $\Sigma_{\mathrm{maj,s},i}(v,T,0)$ are the zero Kelvin elastic scattering cross section of nuclide i and its temperature majorant, respectively. In practice, the relative velocity of the neutron to target, v', is first sampled from Eq. (7) and the sample is accepted or rejected according to the ratio of the zero Kelvin cross section to the majorant. The whole sampling procedure is repeated until a successful sample for v' is obtained.

II.B. TMS Temperature Treatment Technique

The target motion sampling (TMS) temperature treatment technique is a Monte Carlo neutron tracking technique that takes the effect of thermal motion on reaction rates into account on-the-fly during transport calculation. The method was introduced for the first time in English-written journals in Ref. [3] by the authors. It was, however, recently found out that a similar method has been introduced already in 1984 in a Russian journal [5] and that the method is routinely used in at least two Russian Monte Carlo codes [6, 16]. The optimization of the TMS method has been covered in recent articles [4, 8] and the usage of the method together with reaction rate estimators has been studied in Refs. [17, 18]. These references provide a complete description of the method, while only the parts essential to the current article are shortly summarized in the following.

In the TMS tracking scheme the path lengths of neutrons are sampled based on a macroscopic majorant cross section

$$\Sigma_{\mathrm{maj,TMS}}(v) = \sum_i \Sigma_{\mathrm{maj,TMS},i}(v) \tag{9}$$

$$= \sum_i g(v, T_{\mathrm{max},i} - T_{\mathrm{base}}, A_i)\Sigma_{\mathrm{maj},i}(v, T_{\mathrm{max},i} - T_{\mathrm{base}}, T_{\mathrm{base}})\,, \tag{10}$$

[c]Also other ways of dealing with the energy dependence have been introduced: in Ref. [10] a technique based on direct sampling of the secondary neutron velocity has been examined, while in Refs. [11, 12] the correction is done by varying the particle weights. It is also possible to include the effect by using $S(\alpha,\beta)$ tables based on the analytical scattering kernel, which has been covered in sequential Refs. [13–15].

where index i runs over all nuclides in a material zone,

$$\begin{aligned} g(v,T,A_i) &= \int_0^\infty \int_{-1}^1 \frac{v'}{2v} P_{\mathrm{MB}}(V_\mathrm{t},T,A_i) dV_\mathrm{t} d\mu \\ &= \left(1+\frac{1}{2\gamma(T,A_i)^2 v^2}\right) \mathrm{erf}\Big(\gamma(T,A_i)v\Big) + \frac{e^{-\gamma(T,A_i)^2 v^2}}{\sqrt{\pi}\gamma(T,A_i)v} \end{aligned} \tag{11}$$

is the Doppler-broadening integral for constant cross section, erf is the error function, $T_{\mathrm{max},i}$ is the maximum temperature of nuclide i and $\Sigma_{\mathrm{maj},i}$ is the temperature majorant cross section of nuclide i. It should be noted that that the TMS majorant cross sections are otherwise similar to any temperature majorants, but the TMS majorant is additionally multiplied by the g-factor[d].

As a result of the path length sampling, a new collision point candidate is obtained. At each collision point, the target nuclide is first sampled based on the nuclide-wise majorant cross sections. Thus, probability of sampling nuclide i is

$$P_i = \frac{\Sigma_{\mathrm{maj,TMS},i}(v)}{\Sigma_{\mathrm{maj,TMS}}(v)}. \tag{12}$$

Then, the velocity of the nuclide is sampled from distribution in Eq. (7) with T equal to the local temperature at the collision point, and the target-at-rest energy corresponding to the collision v' is calculated. Finally, the collision point is accepted or rejected according to rejection sampling criterion

$$\xi < \frac{g(v,T-T_\mathrm{base},A_i)\Sigma_{\mathrm{tot},i}(v',T_\mathrm{base})}{\Sigma_{\mathrm{maj,TMS},i}(v)} = \frac{g(v,T-T_\mathrm{base},A_i)}{g(v,T_{\mathrm{max},i}-T_\mathrm{base},A_i)} \frac{\Sigma_{\mathrm{tot},i}(v',T_\mathrm{base})}{\Sigma_{\mathrm{maj},i}(v,T_{\mathrm{max},i}-T_\mathrm{base},T_\mathrm{base})}, \tag{13}$$

where ξ is a uniformly distributed random variable on the unit interval. If the sample is rejected, the tracking procedure restarts by sampling of a new path length beginning from the newly rejected collision point. In case the collision point is accepted, a reaction is sampled based on the reaction cross sections at T_base corresponding to the target-at-rest velocity v'. The neutron tracking proceeds according to the sampled reaction.

[d]The multiplication is required for correct modeling of the reaction rates at low energies and is related to the fact that the integral of the distribution from which the target velocities are sampled (Eq. (7)) is greater than unity at low energies. This modification is perhaps the most intuitive in case of potential scatterers with constant low-energy cross sections: these cross sections are increased in the Doppler-broadening process, but the corresponding increase in the reaction rates could not be captured in the TMS transport without multiplying the cross sections by g.

III. Truncation of Thermal Motion in Temperature Majorant Generation

In both of the applications studied in this article, introduced in Sections II.A. and II.B., the temperature majorant cross sections are applied with rejection sampling techniques. When using DBRC, the temperature majorant related rejection criterion is

$$\xi < \frac{\Sigma_{\mathrm{s},i}(v',0)}{\Sigma_{\mathrm{maj,s},i}(v,T,0)} \tag{14}$$

and the rejection sampling criterion of TMS is shown in Eq. (13). These rejection sampling criteria set the one and only basic requirement for the majorant cross section: For the rejection sampling to be valid, the sampled cross sections in Eqs. (13) and (14) shall not exceed the majorant cross section or, in practice, the exceedings must be rare. The majorant exceedings are a sign that part of the target velocity samples (DBRC) or collision points (TMS) may be accepted even though they should be rejected, which introduces bias in the secondary particle distributions of elastic scattering events and the neutron path lengths.

At the same time, the efficiency of the rejection sampling depends strongly on the conservativity of the majorant cross section: if the majorant cross section is large compared to the sampled cross sections, the proportion of accepted samples is small. Hence, determining the cut-offs for thermal motion in the temperature majorant generation is all about balancing between efficiency and accuracy. An optimal majorant would be as small as possible such that the proportion of majorant violations still does not introduce error in the results.

III.A. Traditional Method

The traditional approach for choosing the limits for the target-at-rest velocity v' in the temperature majorant generation has been used in DBRC implementations and in the implementations of the TMS or TMS-like methods in Serpent and PRIZMA [5]. For the DBRC implementations, the exact cut-off condition dates back to an article by Rothenstein, Ref. [19], which started the long journey towards the present DBRC technique. In this article Rothenstein suggested that "a finite range of energies near the neutron energy E can be used in the same manner as in the Doppler broadening code of Cullen", referring to the SIGMA1 code [7]. In the appendix of Ref. [7] it is discussed that since most of the contribution to the Doppler-broadening integral comes from relative velocities x that are close to the neutron velocity y (both dimensionless quantities), the integration can be optimized by limiting the range of x to a narrow region around y. It is, then, shown that if the integration range is chosen as $x \in [y-4, y+4]$, the error from truncation will remain smaller than 0.1 % even if the cross

sections vary by four orders of magnitude in the vicinity of y.

The same cut-off was later on adopted by Becker et al. to determine the energy ranges used in the generation of temperature majorant cross sections for the DBRC [2] method. The integration limits of Cullen can be interpreted as, first, truncating the Maxwellian velocity distribution of the target to a maximum value of

$$V_{\mathrm{t,max}} = h\sqrt{\frac{2k_{\mathrm{B}}\Delta T}{AM_{\mathrm{n}}}} \tag{15}$$

(converted into conventional units) with $h = 4.0$ and, then, determining the range of relative velocities or energies accordingly. Thus, the maximum target-at-rest energy E' corresponds to a head-on collision with $\mu = -1$ in Eq. (4) and the minimum energy is obtained for a parallel collision with $\mu = 1$. For nuclide i and neutron energy E the energy range of thermal motion is bounded by

$$E_{\min}(E, \Delta T, A_i) = \left(\sqrt{E} - h\sqrt{\frac{k_{\mathrm{B}}\Delta T}{A_i}}\right)^2 \tag{16}$$

and

$$E_{\max}(E, \Delta T, A_i) = \left(\sqrt{E} + h\sqrt{\frac{k_{\mathrm{B}}\Delta T}{A_i}}\right)^2. \tag{17}$$

As mentioned in the introduction, the cut-off $h = 4.0$ corresponds to a target energy of 16 $k_{\mathrm{B}}T$.

Needless to say, the original $h = 4.0$ truncation of Cullen is very well justified in the calculation of effective cross sections. Since this cut-off is in any case used when Doppler-broadening the scattering cross sections with NJOY [20], using the same cut-off in the generation of the temperature majorants for DBRC ensures that the kinetics of the elastic scattering events are resolved in consistence with other parts of the neutron transport, specifically reaction rates of scattering events. Hence, the $h = 4.0$ truncation, as adopted by Becker et al., is a logical and safe choice also for the DBRC majorant generation.

In practice it is, however, possible to use also other cut-off conditions for the DBRC majorants without disturbing the neutron transport. The justification for the original truncation, presented in Ref. [7], basically means that with $h = 4.0$ the energy of the target is outside the limits specified by Eqs. (16) and (17) with a probability smaller than 0.1 % even in the worst case scenario when the cross section increases by four orders of magnitude just outside the limits corresponding to the neutron energy E. Since the neutrons end up at these worst-case energies only rarely in normal criticality source calculations and since the error estimate is conservative, the proportion of target samples violating the limits is in practice decades smaller than 0.1 %, i.e. extremely small. When this is combined with the fact that small

errors in the secondary particle distributions have only minor effect on the neutron transport as a whole, reducing the value of the h parameter seems feasible.

Similar reasoning applies also for the TMS majorants with the exception that the errors arising from truncation lead to falsely accepted collision points, which affects the neutron transport in a different way than errors in the secondary neutron distributions. In the implementation of the TMS-like method in PRIZMA the cut-off $h = 3.0$, corresponding to 9 $k_{\mathrm{B}}T$ in terms of energy, has been successfully used [5]. Also this indicates that the conservativity could be, in practice, significantly reduced from the original value of $h = 4.0$ for the TMS majorants.

III.B. Revised Method

The "traditional" way of generating temperature majorant cross sections works perfectly well in practice, but by examining the applications of the temperature majorants, more arguable ways of choosing the energy boundaries can be figured out. In both of the rejection sampling criteria, Eqs. (14) and (13), the value of the sampled cross section depends on v', which is in both cases sampled based on the distribution in Eq. (7). Hence, also the range of sampled cross sections depends on this distribution and, consequently, the energy boundaries in the majorant generation should be based on the distribution in Eq. (7), not the Maxwell-Boltzmann distribution. It is also practical to associate the majorant with a confidence level, $1-Q$, to study the effect of the conservativity of the majorant on the results and performance.

This was the basic idea behind the method introduced in Ref. [8], where different confidence levels were used to determine the maximum target velocities corresponding to a head-on and a parallel collision. However, a more natural way for choosing the boundaries was found after a second consideration. Namely, the confidence level can also be associated directly with the relative velocities such that all possible collision angles are properly taken into account. When defined this way, the physical meaning of the confidence level is much clearer than with the method in Ref. [8].

The two extremes of the relative velocity corresponding to the new energy boundaries, $v'_{\mathrm{min,rev}}$ and $v'_{\mathrm{max,rev}}$, can be resolved by integrating the probability distribution of target velocities, Eq. (7). However, to provide for direct determination of the boundaries for the relative energy, the integration must be done with respect to the relative velocity v' and the cosine between the relative velocity vector and the neutron direction, ν. By comparing Eqs. (7) and (11) it can be seen that the normalization factor C in front of Eq. (7) is, in fact, just the inverse of $g(v, T, A)$. By replacing C with this factor and changing to the previously

mentioned integration variables, equations

$$\begin{aligned} P(v' < z) &= \frac{1}{g(v, \Delta T, A)} \int_0^z \int_{-1}^1 \frac{2}{\sqrt{\pi} v} \gamma^3 v'^3 e^{-\gamma^2 (v^2 + v'^2 - 2vv'\nu)} dv' d\nu \\ &= \frac{1}{g(v, \Delta T, A)} \Big\{ \frac{1}{2\gamma\sqrt{\pi} v^2} \Big(e^{-\gamma^2 (v+z)^2} (z - v) - e^{-\gamma^2 (v-z)^2} (v + z) + 2e^{-\gamma^2 v^2} v \Big) \\ &\quad + (\frac{1}{2} + \frac{1}{4\gamma^2 v^2}) \Big(\mathrm{erfc}\big((v - z)\gamma\big) + \mathrm{erfc}\big((v + z)\gamma\big) - 2\mathrm{erfc}\big(v\gamma\big) \Big) \Big\} \end{aligned} \tag{18}$$

and

$$\begin{aligned} P(v' > z) &= \frac{1}{g(v, \Delta T, A)} \int_z^\infty \int_{-1}^1 \frac{2}{\sqrt{\pi} v} \gamma^3 v'^3 e^{-\gamma^2 (v^2 + v'^2 - 2vv'\nu)} dv' d\nu \\ &= \frac{1}{g(v, \Delta T, A)} \Big\{ \frac{1}{2\gamma\sqrt{\pi} v^2} \Big(e^{-\gamma^2 (v+z)^2} (v - z) + e^{-\gamma^2 (v-z)^2} (v + z) \Big) \\ &\quad + (\frac{1}{2} + \frac{1}{4\gamma^2 v^2}) \Big(\mathrm{erf}\big((v - z)\gamma\big) + \mathrm{erf}\big((v + z)\gamma\big) \Big) \Big\} \end{aligned} \tag{19}$$

are obtained for the tail probabilities. In these equations, erfc is the complementary error function and the dependence of γ on ΔT and A, as specified in Eq. (6), is not explicitly shown for clarity. Furthermore, by using conditions

$$P(v' < v'_{\mathrm{min,rev}}) = \frac{Q}{2} \tag{20}$$

and

$$P(v' > v'_{\mathrm{max,rev}}) = \frac{Q}{2} \tag{21}$$

it is possible to numerically resolve the range of relative velocities corresponding to the confidence level Q, using for example the Newton's method [21]. The relative velocities v' can, further, be converted to the energy range boundaries using Eq. (3).

The small difference between the revised and the traditional energy boundaries in the majorant generation is demonstrated in Figure 2, where the differences in E_{min} and E_{max} between the traditional and the revised majorant with $Q = 1.541 \times 10^{-8}$ are plotted for ^{238}U. The specific Q-value was chosen such that the widths of the energy ranges $E_{\mathrm{max}} - E_{\mathrm{min}}$ are roughly equal at 6.7 eV.

As it can be seen in Figure 2, if the width of the energy range is matched at the low resonance region, the revised method leads to somewhat wider energy ranges than the traditional method at low energies below about 1 eV and at high energies above about 1 keV. While the widths of the energy ranges are similar at the resonance region, the usage of the revised

method shifts both the upper and the lower energy boundaries upwards by about one milli-eV compared to the traditional method.

IV. Results

Serpent version 2.1.15 with a few modifications is used as the testing platform in the calculations performed in Sections IV.B.–IV.D., and the results in Section IV.E. are calculated with a newly-updated version, Serpent 2.1.17. In all of the calculations, the energy threshold for free gas treatment is increased to infinity such that the target velocities are sampled for each elastic scattering event, regardless of the neutron energy. Doppler-broadening rejection correction (DBRC) is applied to ^{238}U between 0.4 eV and 20 keV in all of the calculations. Due to the findings in Ref. [4], usage of DBRC is extended to nuclides ^{95}Mo, ^{108}Pd, ^{131}Xe, ^{145}Nd, ^{147}Pm, ^{152}Sm, ^{239}Pu, ^{240}Pu, ^{242}Pu and ^{241}Am in addition to ^{238}U in the PWR-BU case.

The cross section library is based on JEFF-3.1.1 and has been processed using 0.001 reconstruction tolerance for high accuracy. All of the calculations are performed using 12 OpenMP threads on Intel Xeon X5690 CPUs running at 3.47 GHz.

IV.A. Test Cases

The effect of the temperature majorants on performance is examined in three realistic test cases with slightly different characteristics. The test cases are the same as the thermal systems in Refs. [4] and [17].

Gd-doped Pressurized Water Reactor Assembly (PWR-Gd)

The first "PWR-Gd" case involves a 17x17 PWR fuel assembly with 16 Gadolinium-doped fuel rods in an infinite two dimensional lattice. The geometry and material definitions of the fuel assembly are from a NEA benchmark [22]. The only differences to the benchmark specifications are related to temperatures: the moderator temperature is risen to 600 K for simplicity and the originally flat temperature profiles of the fuel rods are replaced with 3-step distributions such that the pellets are divided into three equi-thick annular regions with temperatures 600 K, 900 K and 1200 K from outside in.

PWR-Gd Assembly at 40 MWd/kgU burnup (PWR-BU)

The second case is abbreviated "PWR-BU" and features the previously introduced "PWR-Gd" bundle irradiated to 40 MWd/kgU burnup. The irradiated material compositions were

obtained by running a separate burnup calculation using Serpent 2.1.14. The resulting compositions contain 241 actinide and fission product nuclides with cross sections available in the data libraries.

High Temperature Gas Cooled Reactor System (HTGR)

The "HTGR" test case consists of TRISO particles within graphite matrix in an infinite three dimensional lattice. The specifications of the TRISO particles and the composition of the graphite matrix are based on a NEA benchmark for HTGR fuel depletion [23], and the lattice pitch is 0.16341 cm. The fuel kernel in the spherical TRISO particles is divided in two equally thick parts such that the innermost 0.0125 cm is at 1800 K temperature and the outer layer is at 1200 K. The temperature of all other materials is 1200 K.

IV.B. Traditional Versus Revised Majorant

Since the revised way of choosing the majorant energies differs substantially from the traditional way, comparison of the two different majorant types must be done indirectly. Probably the best way to judge, which of the two methods performs better in neutron transport is through the sampling efficiencies and sampling violations: if majorant A leads to a higher average sampling efficiency with the same or a lower proportion of majorant exceedings than majorant B, then A can be considered superior to B.

Since the traditional majorant with original SIGMA1 cutoffs is very conservative and, consequently, the majorant exceedings are very rare, it is practical to modify the majorant for the following study. The original multiplier $h = 4.0$ in the cut-off condition of the traditional majorant (Eqs. (15), (16) and (17)) is replaced by $h = 3.0$, which makes the majorant less conservative.

Before the efficiencies can be compared, the confidence level $1 - Q$ must be determined for the revised majorant such that the proportion of majorant exceedings becomes roughly equal to that from calculations with the modified traditional majorant. The task is complicated by the fact that this Q-parameter may differ between the systems and it also depends on whether the proportion of TMS majorant or DBRC majorant exceedings is considered. Reason for this is that while the Q parameter determines the proportion of sampled relative velocities outside the energy range used in the majorant generation, the proportion of majorant exceedings depends also on the cross sections in the rejection sampling criteria. The cross sections, for their part, depend on whether scattering cross sections (DBRC) or total cross sections (TMS) are considered, the nuclides for which the methods are applied, the temperatures of the cross

sections and, additionally, the neutron flux spectrum affects the energies at which these cross sections are applied in the rejection sampling. The Q parameters were determined for each of the three different test cases with trial and error. To rationalize the amount of work, Q parameters were only determined at an accuracy of 10^{-6}.

The results of the calculations are provided in Tables I and II for TMS and DBRC, respectively. For both of the studies, the average sampling efficiencies and proportions of majorant exceedings $P_{\mathrm{err,\ maj}}$ are provided. The statistical deviations of the sampling efficiencies are negligible (< 0.01 %) and are, therefore, not shown in the tables. In addition, the proportions of target velocity samples outside the energy range used in the TMS majorant generation are provided for the TMS calculations. The proportion of target velocity samples for which the target-at-rest energy E' is below $E_{\min}(E)$ is denoted with $P_{\mathrm{err,low}}$ and, correspondingly, the proportion of samples above $E_{\max}(E)$ is $P_{\mathrm{err,high}}$. It should be noted that the proportion of majorant exceedings is significantly lower than the sum of boundary violations, because the cross section corresponding to the "illegal" target velocity sample is only rarely larger than the majorant at resonance energies, where a significant proportion of the interactions takes place. At low energies with $1/v$ cross sections the situation is different and samples violating the lower energy boundary always result in majorant exceedings. Number of active neutron histories was 500 million in all of the calculations.

The results for the TMS calculations, presented in Table I, show that the revised majorant results in slightly higher TMS sampling efficiencies with a lower proportion of erroneous samples than the traditional majorant. The increase in efficiency should also affect the transport calculation times, but the differences are small compared to the uncertainties associated with these measures. The main idea of the revised majorant can be seen in the proportions of upper and lower majorant boundary violations: for the revised majorant the proportion of velocity samples below the lower boundary is equal to the proportion of samples that violated the upper boundary, while the distribution of erroneous samples is non-symmetrical for the traditional majorant.

Instead, the results of the DBRC calculations in Table II show no practical difference between the traditional and the revised majorant. The proportions of erroneous samples are the same within statistical accuracy and also the DBRC sampling efficiencies are practically equal for both of the majorant types.

It should be noted that also the majorant generation times affect the overall performance of the different majorant types. As can be seen in the Tables I and II, the majorant generation times for the revised majorant are about 2–7 times higher than for the traditional majorant,

since the revised boundaries are more complicated to calculate. In typical calculations with good statistics the 0.7 %–1.5 % increase in the TMS sampling efficiency is expected to compensate the extra time spent in the majorant generation, because most of the calculation time is in any case spent in the neutron transport. However, in calculations with poor statistics the traditional majorant may actually outperform the revised majorant. The overhead in the majorant generation could be at least somewhat reduced by optimizing the algorithm used in the calculation of the revised majorant boundaries.

IV.C. Optimal Level of Conservativity in TMS Applications

Determining an optimal level of conservativity for the majorant cross section is problematic, since on the other hand one would like to use as small, or as non-conservative, majorant as possible to get high efficiency, but on the other hand using of a too tight cut-off condition for the thermal motion will introduce significant error in the calculations, which of course should be avoided by all means. Experimenting with the majorants also has shown that the optimal level of conservativity is problem-dependent and, to avoid errors, the determination of the majorant should be based on a realistic transport problem that is as sensitive to the majorant violation errors as possible.

An unambiguous worst-case-scenario is impossible to determine, but some clue on the properties of the problem can be obtained based on previous experience. First of all, the majorant violations tend to have the most effect on the neutron spectrum and k_{eff} in systems in which the neutrons experience a lot of collisions with the fuel material at the energy region of resolved resonances. A good example of such a system is the HTGR test case, introduced in Section IV.A., which involves very small fuel particles dispersed in a graphite matrix[e]. Second, while the temperature difference between T_{base} and the maximum temperature of the system has only moderate effect on the proportion of majorant violations, a larger temperature difference leads to more significant violations, which are expected to have stronger impact on the transport. As 3000 K is usually considered the maximum temperature required in reactor physical analysis, this is chosen as the fuel temperature in the HTGR system. To maximize the temperature difference, the cross sections are kept at $T_{\text{base}} = 0$ K temperature, which also enables re-using of the sampled velocities in the solution of scattering kinetics [4]. Thus,

[e]Since this system is in practice a quasi-homogeneous mixture of moderator and fuel, the probability of a neutron to interact with the fuel material during the slowing-down process is very high compared to, for instance, LWR geometries. In addition, the fact that the moderator atoms in graphite are relatively heavy ($A_{\text{C}} \approx 12$) increases the number of scattering events a neutron experiences during the process compared to lighter moderators like hydrogen. This increases the probability of a neutron to end up at energies corresponding to resonances in the fuel material at some point of the slowing-down process and, thus, makes the interactions more probable on average.

DBRC is not required in these calculations.

The effect of the majorant conservativity on the accuracy of the TMS method is studied in this HTGR system with 3000 K fuel. For the sake of simplicity, the main comparison is based on different k_{eff} estimates that should all agree with the reference solution within statistics as long as the transport is physically valid. The three k_{eff} estimators are

1. the "analog estimator", which is the ratio of source weights in subsequent neutron generations

2. the "implicit estimator", defined

$$k_{\text{eff,imp}} = \frac{\overline{\nu} R_{\text{f}}}{R_{\text{f}} + R_{\text{c}} - R_{(\text{n,xn})} + R_{\text{L}}} , \tag{22}$$

   where $\overline{\nu}$ is the average number of neutrons emitted in a fission, R_f, R_c and R_L are fission, total capture and leakage rates, respectively, and

$$R_{(\text{n,xn})} = \sum_y (y-1) R_{(\text{n,yn})} \tag{23}$$

   is the neutron production rate from (n,xn) reactions.

3. the "collision estimator", which is the ratio of $\overline{\nu} R_{\text{f}}$ to the neutron source size.

In addition, the results are confirmed by comparing the neutron flux spectra of relevant calculations to the reference solution.

The calculations were run using 500 million active neutron histories. The results are provided in Figure 3 for the revised majorant and in Figure 4 for the traditional majorant. The reference value value of k was calculated using 2.5 billion neutron histories and NJOY-broadened cross sections [20]. The neutron flux spectra of two relevant calculations with revised majorants are compared to the reference in Figure 5. The neutron spectra are normalized to constant total flux.

In Figure 3 it can be seen that all three k-estimators agree within statistics with each other and with the reference solution as long as $Q \leq 10^{-4}$. With higher values the k_{eff} estimators deviate from each other significantly and also the k_{eff} values are no longer in agreement with the reference solution. The same effect can be seen in Figure 5: with $Q = 10^{-4}$ the neutron flux spectra are in perfect agreement, but with $Q = 3.2 \times 10^{-4}$ a small positive bias is observed in the lower epithermal region. Thus, it seems that the optimal value for the Q parameter is near $Q = 10^{-4}$. What comes to the results of the traditional majorant in Figure 4, the optimal

boundary is slightly harder to recognize, but side-by-side comparison of neutron spectra and k reveals that $h = 2.8$ is the lowest acceptable value.

IV.D. Optimal Level of Conservativity in DBRC Applications

The same system that was used in the previous section suits also very well in the studying of the effect of the majorant conservativity on the functionality of the DBRC method. As the total effect of the Doppler-Broadening Rejection Correction on the eigenvalue is about 1500 pcm, it is hard to figure out a practical reactor physical problem that would be more sensitive to the correct functionality of the correction.

All the cross sections are NJOY-originated, i.e. no TMS method nor the Doppler preprocessor of Serpent is used in the calculations [24]. Eigenvalue results of the calculations are provided in Figures 6 and 7 for the revised and the traditional majorant, respectively.

Results indicate that the conservativity of the majorant can be decreased even lower than in the TMS case before the effect of the majorant violations on k_{eff} can be recognized. With the revised majorant the highest Q value for which the eigenvalue estimators are still correct is $Q = 3.2 \times 10^{-3}$ and for the traditional majorant the smallest acceptable value seems to be $h = 2.3$. These results were also confirmed by comparing the neutron spectra, which agreed with the reference solution within statistical deviation. The flux comparison for the revised majorant is shown in Figure 8.

IV.E. Performance Results

On basis of the previous results, presented in Sections IV.B.– IV.D., the revised majorant type was chosen as the default majorant in Serpent version 2.1.17 for both TMS and DBRC majorants. The implementation of the traditional majorants was, however, left in the code as a compiler option to provide for easy experimenting in the future. Value of $Q = 2.0 \times 10^{-5}$ was, conservatively, chosen as the default confidence level in the majorant generation for the TMS. In case the traditional majorant generation is activated, the default value for the temperature cut-off is, again conservatively, the same as in the PRIZMA code, $h = 3.0$. It was decided to use the same default values of Q and h also for the DBRC majorants even though the previous results indicate that also less conservative majorants could be used without compromising the accuracy of important reactor physical results. As the computational overhead from DBRC is relatively small, it was decided to be rather safe than sorry in this matter.

In the previous articles on the TMS method [4, 8, 17], the performance of the method has been compared to standard Serpent calculations with reduced optimization, i.e. Serpent

calculations that have been purposely slowed down. This choice was made because Serpent with full optimization takes advantage of pre-calculated macroscopic cross sections and this kind of optimization cannot be used together with the TMS method. Thus, if the performance of TMS was compared to Serpent with full optimization, it would be self-evident that a significant part of the overhead would be caused by the lack of pre-calculated macroscopic cross sections, especially in problems involving hundreds of nuclides. However, the slowing-down of the reference calculations has its own downsides as it was noticed for example in [4], where the TMS method appeared even faster than the reference in a couple of cases. This kind of results make little sense as the TMS should always increase the computational effort compared to conventional transport in fair a comparison due to the sub-unitary sampling efficiency. To get consistent results, it was decided to make an "unfair" comparison for the TMS in the current article and use full optimization in the reference calculations. However, calculation times are provided also for corresponding calculations with reduced optimization, optimization mode 2 to be precise [25]. The performance comparison for the DBRC calculations is more straightforward, since DBRC works inherently with full optimization.

The temperature of the cross sections, T_{base}, was chosen as the minimum temperature of each nuclide in the system in the TMS calculations. Performance measures of the calculations are provided in Table III. The Table also includes results and figures-of-merit (FOM) for two estimators in the TMS cases. First of these estimators is for the total (energy-integrated) capture rate in the corner rods (PWR-Gd and PWR-BU cases) or all fuel material (HTGR case). The second estimator calculates the capture rate around the 6.7 eV resonance of ^{238}U ($6.5 - 6.9$ eV), which was found to be problematic in Reference [17] when using the TMS[f].

The TMS results show that by reducing the conservativity of the majorant from the original $h = 4.0$ value it is possible to save 8–23 % of the transport calculation time without affecting the results. This applies also for the neutron flux spectra and the results of the reaction rate estimators, which are omitted here for the sake of simplicity. The performance is somewhat better for the revised majorant with the chosen conservativity parameters h and Q, but as it can be seen in the proportions of majorant-violating samples, $P_{\text{err,maj,TMS}}$, the revised majorant with $Q = 2 \times 10^{-5}$ also leads to a slightly larger fraction of majorant failures. With the newly implemented revised majorant the overhead from using TMS, unfairly compared to Serpent 4 with full optimization, is 1.24 in the PWR case, 1.18 in the HTGR case and 12.33 in the PWR-BU case.

[f]It was found in [17] that the variances and, consequently, also the Figures-of-Merit for all estimators including the flux estimator are significantly affected by the usage of the TMS method near strong resonances.

The majorant cross section has significantly less effect on the performance of the DBRC method. In Serpent the overhead from the DBRC method is about 4-8 % in these test cases when using the traditional temperature majorant with $h = 4.0$, as suggested by the developers of the DBRC method. By reducing the conservativity of the majorant cross section, this overhead can be reduced by a couple of percents.

It should also be noted that the performance of the TMS method with the old $h = 4.0$ majorant has somewhat improved from the previous results presented in [4]. This is due to many small changes in the implementation, perhaps most important of which was changing from a point-wise to a histogram representation for the temperature majorant cross sections.

V. Summary and Conclusions

In this article, a revised approach for generation of the temperature majorant cross sections was first introduced, and the revised majorants were compared to those generated using the traditional approach. An optimal cut-off condition was sought by applying TMS and DBRC in a reactor system in which the majorant violations are expected to have very large effect on the transport calculation. After finding optimal values for the f and Q parameters, which affect the conservativity of the traditional and revised type majorants, the temperature majorant generation in Serpent 2.1.17 was optimized according to the new results. Finally, the updated version was applied in three thermal reactor systems with different characteristics to estimate the effects of the updated temperature majorants on the performance of the transport calculation.

The difference between the traditional and revised majorants was rather small: In TMS applications the revised majorant resulted in 0.7–1.5 % larger sampling efficiencies than the traditional majorant with practically the same proportion of majorant violations. Instead, no practical difference between the two majorant types was observed in DBRC applications. Thus, switching to more complicated revised majorants does not make any difference in DBRC implementations, but with TMS method the introduction of the revised truncation can bring a slight increase in the performance of the transport calculation. In short calculations the benefit from using the revised boundaries may be lost due to more time consuming majorant generation in the pre-processing phase, but in typical calculations with good statistics the usage of the revised majorants pays off.

What comes to the TMS calculations, the results showed that the calculation times are reduced by about 8–23 % when applying the suggested, less conservative cut-off conditions. In calculations involving only a few resonance absorbers the overhead from using the TMS

method is well-feasible, about 1.2-1.3. However, with numerous temperature-dependent nuclides the overhead compared to a Serpent calculation with full optimization increases to about 12. Most of this slow-down comes from the fact that Serpent normally pre-calculates the macroscopic cross sections and this kind of optimization cannot be applied together with the TMS method as long as all of the nuclides are treated temperature-dependently.

Switching to the less-conservative temperature majorants decreased also the computational overhead from the DBRC method significantly. Nevertheless, since the original overhead from using DBRC in Serpent was only 4–8 %, the overall gain in performance remained small.

It should be kept in mind that reducing the conservativity of the temperature majorants introduces systematic bias in the transport calculation. According to the results of the current study the chosen values for Q and h are conservative enough for the errors to remain statistically insignificant in practical calculations with realistic reactor systems. Thus, the results should be fine as long as for example neutron flux, reaction rates, cross sections or any derived parameter like k is calculated using criticality source simulation.

The same does not necessarily apply when studying very narrow energy regions, for example using mono-energetic external neutron sources. The biases from majorant violations are concentrated at narrow energy intervals in the vicinity of strong resonances, and these errors are lost in the background when integrating over wider intervals. However, with very narrow energy binning and certain energies the bias may become significant. When using mono-energetic neutron sources this kind of errors are, luckily, easy to recognize automatically by analyzing the proportion of majorant violations. In case the proportion seems suspiciously large, it is possible to increase the conservativity of the majorant via user input.

In the light of the results presented above, it seems in any case reasonable to provide the users of Monte Carlo codes with a possibility to manipulate the conservativity of the DBRC and TMS majorants.

Acknowledgments

This work was partly funded from the NUMPS project of the Finnish Academy the KÄÄRME project under the Finnish Research Programme on Nuclear Power Plant Safety SAFIR2014.

REFERENCES

[1] MCNP X-5 Monte Carlo Team, "MCNP — a General Monte Carlo N-Particle Transport Code," Version 5, LA-UR-03-1987, Los Alamos National Laboratory (2003).

[2] B. Becker, R. Dagan and G. Lohnert, "Proof and implementation of the stochastic formula for ideal gas, energy dependent scattering kernel," *Ann. Nucl. Energy*, **36**, 470–474 (2009).

[3] T. Viitanen and J. Leppänen, "Explicit treatment of thermal motion in continuous-energy Monte Carlo tracking routines", *Nucl. Sci. Eng.*, **171**, 165-173 (2012).

[4] T. Viitanen and J. Leppänen, "Target Motion Sampling Temperature Treatment Technique With Elevated Basis Cross Section Temperatures", *Nuc. Sci. Eng.*, Accepted

[5] V.N. Ogibin and A.I. Orlov, "Majorized cross-section method for tracking neutrons in moving media", *Voprosy Atomnoj Nauki i Techniki, Metodoki i Programmy*, **2(16)**, 6–9 (1984), *In Russian.*

[6] Y.Z. Kandiev et al., "PRIZMA Status", *Proc. SNA+MC2013.* Paris, France, 27–31 October, 2013.

[7] D.E. Cullen and C.R. Weisbin, "Exact Doppler Broadening of Tabulated Cross Sections", *Nucl. Sci. Eng.*, **60**, 199–229 (1976).

[8] T. Viitanen and J. Leppänen, "Optimizing the Implementation of the Explicit Treatment of Thermal Motion — How Fast Can It Get?", *Proc. M&C 2013*, Sun Valley, ID, May 5–9, 2013.

[9] R.R. Coveyou, R.R. Bate and R. K. Osborn, "Effect of Moderator Temperature upon Neutron Flux in Infinite, Capturing Medium", *J. Nucl. Energy*, **2**, 153–167 (1956).

[10] E.E. Sunny and W.R. Martin, "On-The-Fly Generation of Differential Resonance Scattering PDF", *Trans. Am. Nucl. Soc.*, **107**, 1124–1127 (2012).

[11] D. Lee, K. Smith and J. Rhodes, "The Impact of ^{238}U Resonance Elastic Scattering Approximations on Thermal Reactor Doppler Reactivity", *Ann. Nucl. Energy*, **36**, 274–280 (2009).

[12] T. Mori and Y. Nagaya, "Comparison of Resonance Elastic Scattering Models Newly Implemented in MVP Continuous-Energy Monte Carlo Code", *J. Nucl. Sci. Tech.*, **46**, 793–798 (2009).

[13] M. Ouisloumen and R. Sanchez, "A Model for Neutron Scattering Off Heavy Isotopes That Accounts for Thermal Agitation Effects", *Nucl. Sci. Eng.*, **107**, 189–200 (1991).

[14] W. Rothenstein, "Proof of the formula for the ideal gas scattering kernel for nuclides with strongly energy dependent scattering cross sections", *Ann. Nucl. Energy*, **31**, 9–23 (2004).

[15] R. Dagan, "On the use of $S(\alpha, \beta)$ tables for nuclides with well pronounced resonances", *Ann. Nucl. Energy*, **32**, 367–377 (2005).

[16] A.N. Ivanov and N.V. Ivanov, "Accounting for the thermal motion of atoms in media in neutron transport simulation by the Monte Carlo method", *Journal Voprosy atomnoj nauki i techniki, Matematicheskoe modelirovanie physicheskikh processov*, **4**, 25-32 (2003).

[17] T. Viitanen and J. Leppänen, "Effect of the Target Motion Sampling Temperature Treatment Method on the Statistics and Performance", *Proc. SNA+MC2013*. Paris, France, 27–31 October, 2013.

[18] T. Viitanen, J. Leppänen and B. Forget, "Target Motion Sampling Temperature Treatment Technique with Track-length Estimators in OpenMC - Preliminary results", PHYSOR 2014, Kyoto, Japan, 28th September – 3rd October, 2014 (submitted).

[19] W. Rothenstein, "Effect of Upscattering by Heavy Nuclides on Doppler Changes of Resonance Absorption", *Proc. ENS Conference 1994*, Tel Aviv, Israel, 23–26 January, 1994.

[20] R. E. MacFarlane and D. W. Muir, "NJOY99.0 Code System for Producing Pointwise and Multigroup Neutron and Photon Cross Sections from ENDF/B Data," PSR-480, Los Alamos National Laboratory (2000).

[21] E. Kreyszig, "Advanced Engineering Mathematics", 8th edition, John Wiley & Sons inc., New York, (1999).

[22] B. Roque et al., "Specification for the Phase 1 of a Depletion Calculation Benchmark devoted to Fuel Cycles", NEA/NSC/DOC(2004)11, OECD/NEA (2004).

[23] M.D. DeHart and A. P. Ulses, "Benchmark Specification for HTGR Fuel Element depletion", NEA/NSC/DOC(2009)13, Nuclear Energy Agency, Organization for Economic Cooperation and Development (2009).

[24] J. Leppänen and T. Viitanen, "New Data Processing Features in the Serpent Monte Carlo Code", *J. Korean Phys. Soc.*, **59**, 1365–1368 (2011).

[25] J. Leppänen and A. Isotalo, "Burnup Calculation Methodology in the Serpent 2 Monte Carlo Code", *Proc. PHYSOR-2012*, Knoxville, TN, 15–20 April, 2012.

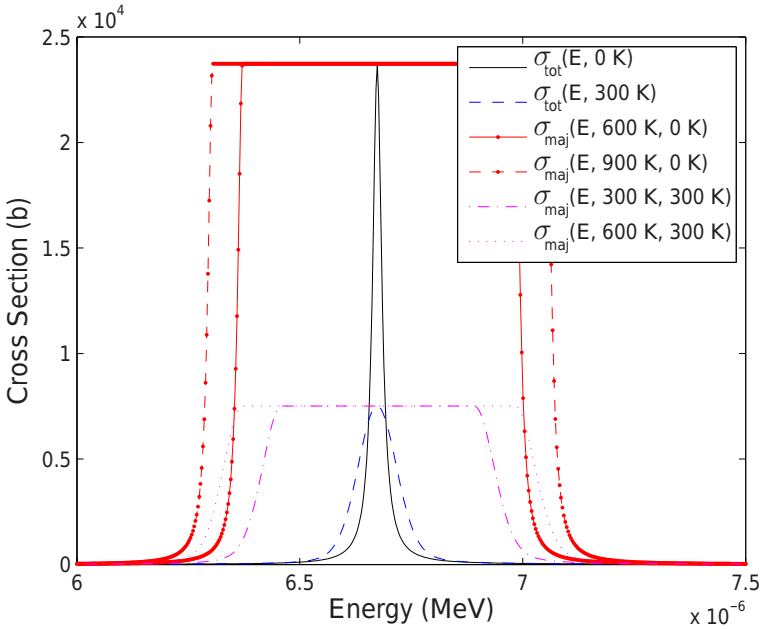

Figure 1 *Majorant cross sections for different basis temperatures T_{base} (0 K and 300 K) and temperature differences (300 K, 600 K and 900 K) for the total cross section of ^{238}U around the 6.7 eV resonance.*

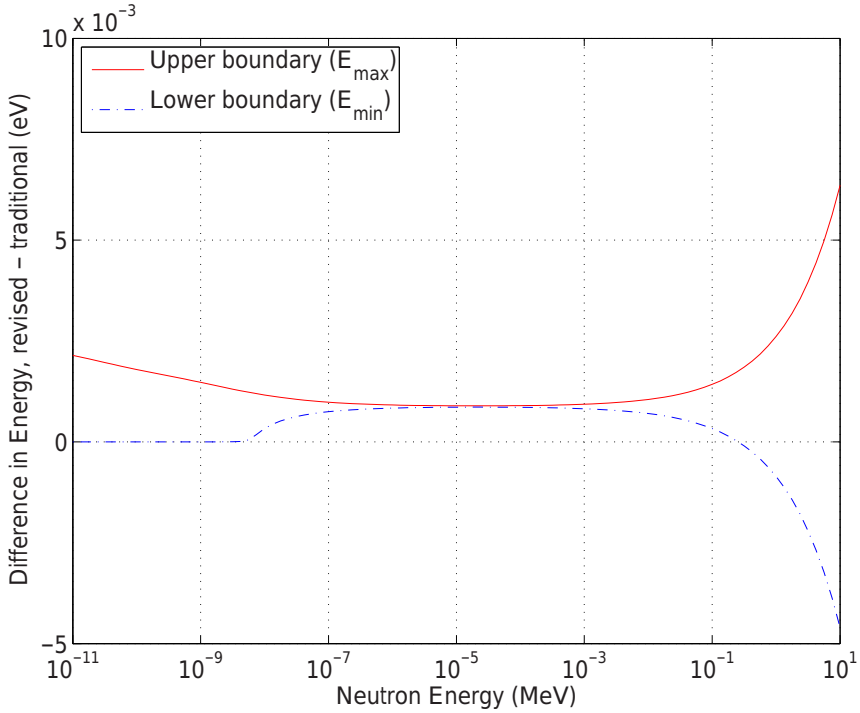

Figure 2 *The energy ranges are defined differently for the revised and the traditional majorant.*

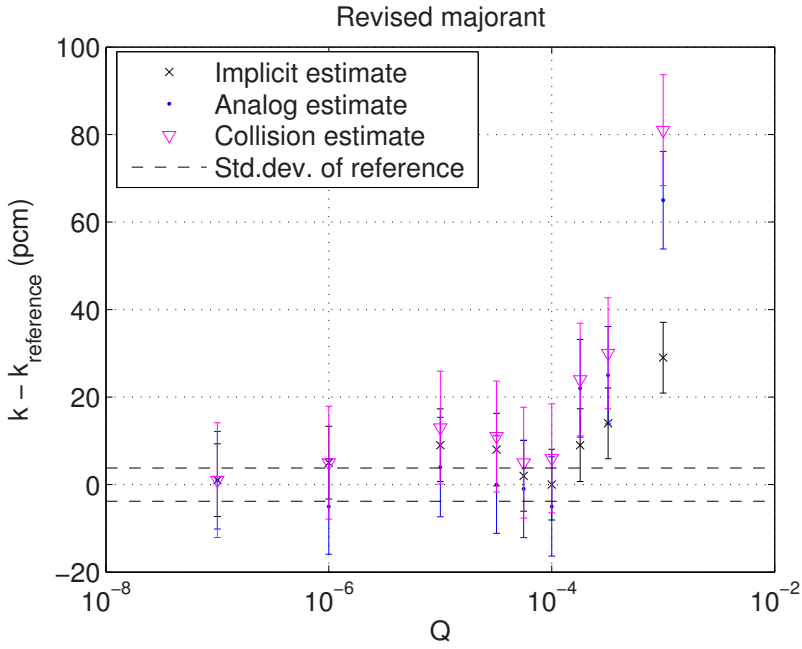

Figure 3 *Effect of the conservativity of the TMS majorant on three* k_{eff} *estimators of a HTGR system. The effect is studied for the revised majorant and, thus, the conservativity is manipulated through the Q parameter. The error bars correspond to two standard deviations, 2* σ*.*

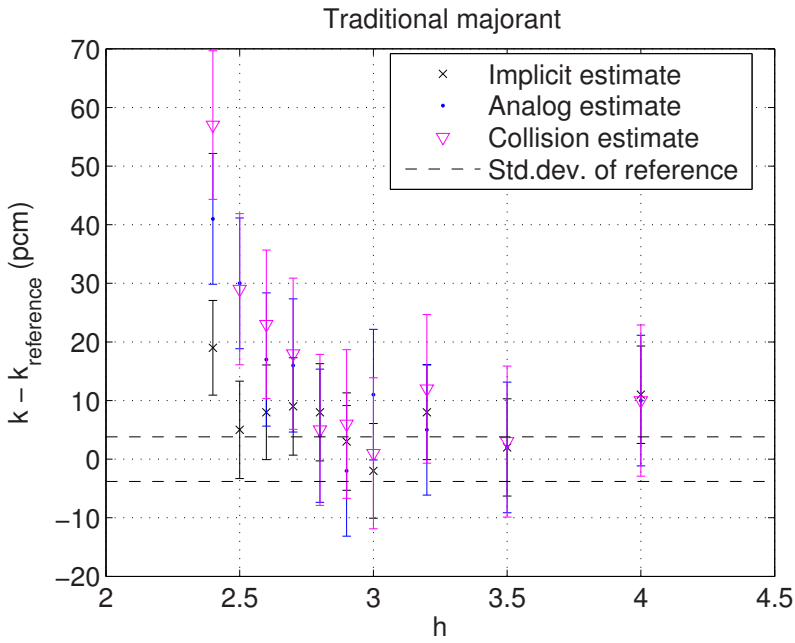

Figure 4 *Effect of the conservativity of the TMS majorant on three different k_{eff} estimators of a HTGR system. The conservativity is manipulated through the h parameter of the traditional majorant.*

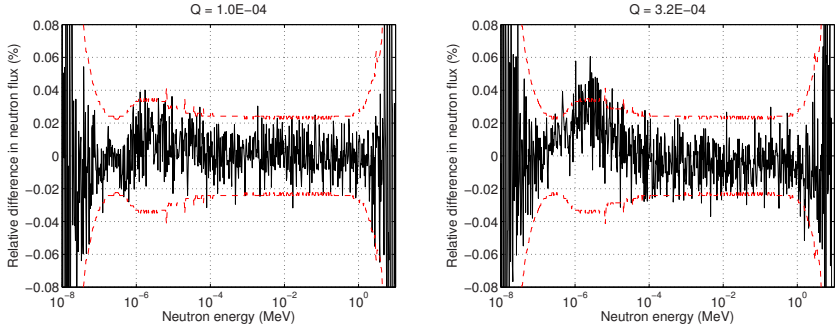

Figure 5 *Comparison of neutron flux spectra between two TMS calculations and NJOY-based reference solution. With Q=1E-4 (left) the flux spectrum corresponds to the reference, but with Q=3.2E-4 (right) significant differences can be recognized. The dashed line corresponds to two standard deviations.*

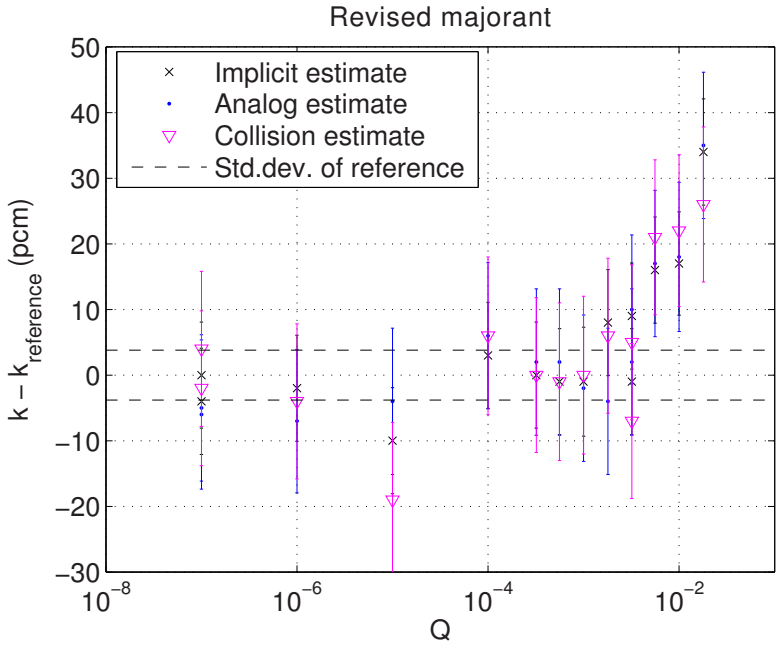

Figure 6 *Effect of the conservativity of the revised DBRC majorant on three k_{eff} estimators of a HTGR system.*

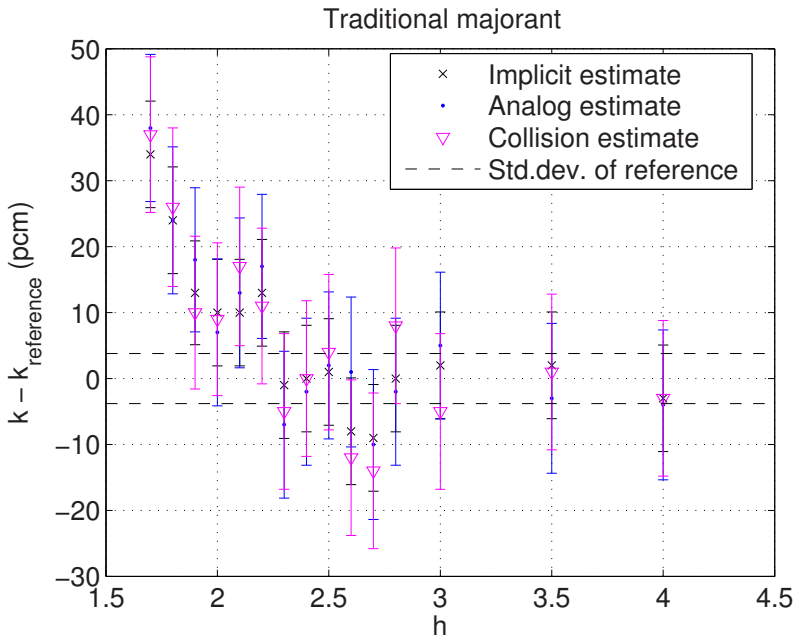

Figure 7 *Effect of the conservativity of the traditional DBRC majorant on three different* k_{eff} *estimators of a HTGR system.*

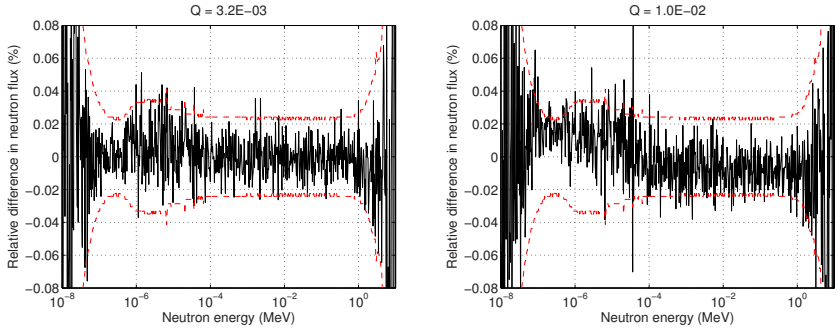

Figure 8 *Comparison of neutron flux spectra between two DBRC calculations and NJOY-based reference solution. With h=3.2E-3 (left) the flux spectrum corresponds to the reference, but with h=1.0E-2 (right) significant differences can be recognized.*

Table I *Performance comparison between traditional and revised majorant when applying TMS method in three thermal systems.*

	PWR-Gd	PWR-BU	HTGR
TMS with traditional majorant, $h = 3.0$			
Majorant generation time (s)	1.08	343.05	0.77
Transport time (h)	3.15	34.62	9.14
k_{eff}	1.15513 ± 6 pcm	0.93453 ± 6 pcm	1.20196 ± 6 pcm
TMS sampling efficiency (%)	51.7	50.4	47.3
$P_{\text{err,maj,TMS}}$	4.02E-07 ± 9E-09	4.43E-07 ± 9E-09	5.13E-07 ± 1E-08
$[P_{\text{err,low}}, P_{\text{err,high}}]$	[9.9E-06, 1.3E-05]	[9.8E-06, 1.3E-05]	[9.3E-06, 1.5E-05]
TMS with revised majorant			
Q	1.8E-05	1.8E-05	1.8E-05
Abs. / Rel. majorant generation time (s/-)	7.92 / 7.36	772.40 / 2.25	3.88 / 5.03
Abs. / Rel. transport time (h/-)	3.11 / 0.99	35.02 / 1.01	8.56 / 0.94
k_{eff}	1.15524 ± 6 pcm	0.93462 ± 6 pcm	1.20206 ± 6 pcm
TMS sampling efficiency (%)	53.0	51.9	48.0
$P_{\text{err,maj,TMS}}$	3.76E-07 ± 8E-09	3.89E-07 ± 8E-09	4.65E-07 ± 1E-08
$[P_{\text{err,low}}, P_{\text{err,high}}]$	[9.0E-06, 9.0E-06]	[8.5E-06, 8.5E-06]	[9.0E-06, 9.1E-06]

Table II *Performance comparison between traditional and revised majorant when applying DBRC method in three thermal systems.*

	PWR-Gd	PWR-BU	HTGR
DBRC with traditional majorant, $h = 3.0$			
Majorant generation time (s)	0.12	18.39	0.09
Transport time (h)	2.35	4.76	6.98
k_{eff}	1.15515 ± 6 pcm	0.93455 ± 6 pcm	1.20200 ± 5 pcm
DBRC sampling efficiency (%)	5.56	5.63	4.49
$P_{\text{err,maj,DBRC}}$	10.0E-08 ± 3E-09	9.9E-08 ± 3E-09	6.0E-08 ± 3E-09
DBRC with revised majorant			
Q	2.2E-05	2.1E-05	2.1E-05
Abs. / Rel. majorant generation time (s/-)	0.64 / 5.26	38.11 / 2.07	0.50 / 5.69
Abs. / Rel. transport time (h/-)			
k_{eff}	1.15512 ± 6 pcm	0.93447 ± 6 pcm	1.20200 ± 5 pcm
DBRC sampling efficiency (%)	5.57	5.63	4.47
$P_{\text{err,maj,DBRC}}$	10.3E-08 ± 3E-09	9.8E-08 ± 3E-09	6.2E-08 ± 3E-09

Table III *Final performance results for three test cases. The relative (rel.) values are calculated with respect to the "Reference" calculation, an ordinary Serpent calculation with DBRC and full optimization. The errors correspond to one sigma.*

	PWR-Gd	PWR-BU	HTGR
Number of active neutron histories	10^9	5×10^8	5×10^8
Reference, h=4.0			
k_{eff}	1.15523	0.93453	1.20248
Δk_{eff} (pcm)	2	2	4
Transport time (h)	5.2	2.7	7.5
Memory requirement (GB)	3.4	91.2	1.1
$P_{\text{err,maj,DBRC}}$	3.3E-11	0.0E+00	0.0E+00
FOM, Total Capture Rate ($\frac{1}{\text{s}}$)	4.1E+04	5.4E+04	1.4E+06
FOM, Capture Rate Around 6.7 eV ($\frac{1}{\text{s}}$)	9.2E+02	8.7E+02	1.1E+05
Reference with reduced optimization			
Abs. / Rel. Transport time (h/-)	7.2 / 1.39	24.4 / 9.04	10.5 / 1.40
Reference without DBRC			
$k - k_{\text{ref}}$ (pcm)	134 ± 3	135 ± 3	717 ± 5
Abs. / Rel. Transport time (h/-)	4.9 / 0.94	2.5 / 0.92	7.2 / 0.97
TMS with Traditional Majorant, h=4.0			
$k_{\text{TMS}} - k_{\text{ref}}$ (pcm)	1 ± 3	0 ± 3	1 ± 5
Abs. / Rel. Transport time (h/-)	7.2 / 1.39	43.0 / 15.96	10.1 / 1.35
Abs. / Rel. Memory requirement (GB/-)	2.5 / 0.72	34.0 / 0.37	1.0 / 0.91
TMS Sampling efficiency (%)	39.3	38.1	38.1
$P_{\text{err,maj,TMS}}$	3.4E-10	3.9E-10	2.4E-10
Abs. / Rel. FOM, Tot. Capt. ($\frac{1}{\text{s}}$/-)	2.9E+04 / 0.72	3.2E+03 / 0.06	1.0E+06 / 0.74
Abs. / Rel. FOM, Capt. Around 6.7 eV ($\frac{1}{\text{s}}$/-)	4.6E+02 / 0.50	3.7E+01 / 0.04	7.3E+04 / 0.65
TMS with Traditional Majorant, h=3.0			
$k_{\text{TMS}} - k_{\text{ref}}$ (pcm)	-2 ± 3	3 ± 3	7 ± 5
Abs. / Rel. Transport time (h/-)	6.6 / 1.26	34.4 / 12.76	9.2 / 1.22
Abs. / Rel. Memory requirement (GB/-)	2.5 / 0.72	34.0 / 0.37	1.0 / 0.91
TMS Sampling efficiency (%)	51.7	50.4	47.4
$P_{\text{err,maj,TMS}}$	3.9E-07	4.5E-07	4.9E-07
Abs. / Rel. FOM, Tot. Capt. ($\frac{1}{\text{s}}$/-)	3.0E+04 / 0.74	4.0E+03 / 0.07	1.2E+06 / 0.86
Abs. / Rel. FOM, Capt. Around 6.7 eV ($\frac{1}{\text{s}}$/-)	4.8E+02 / 0.52	5.1E+01 / 0.06	8.5E+04 / 0.75
TMS with Revised Majorant, $Q = 2 \times 10^{-5}$			
$k_{\text{TMS}} - k_{\text{NJOY}}$ (pcm)	3 ± 3	1 ± 3	-1 ± 5
Abs. / Rel. Transport time (h/-)	6.4 / 1.24	33.2 / 12.33	8.8 / 1.18
Abs. / Rel. Memory requirement (GB/-)	2.5 / 0.72	34.0 / 0.37	1.0 / 0.91
TMS Sampling efficiency (%)	53.2	52.3	48.2
$P_{\text{err,maj,TMS}}$	4.2E-07	4.9E-07	5.2E-07
Abs. / Rel. FOM, Tot. Capt. ($\frac{1}{\text{s}}$/-)	3.1E+04 / 0.75	3.9E+03 / 0.07	1.2E+06 / 0.85
Abs. / Rel. FOM, Capt. Around 6.7 eV ($\frac{1}{\text{s}}$/-)	4.9E+02 / 0.53	4.8E+01 / 0.06	8.4E+04 / 0.74
DBRC with Traditional Majorant, h=3.0			
$k - k_{\text{ref}}$ (pcm)	-1 ± 3	2 ± 3	-10 ± 5
Abs. / Rel. Transport time (h/-)	5.0 / 0.96	2.6 / 0.98	7.4 / 0.99
$P_{\text{err,maj,DBRC}}$	9.0E-08	1.0E-07	5.1E-08
DBRC with Revised Majorant, $Q = 2 \times 10^{-5}$			
$k_{\text{TMS}} - k_{\text{NJOY}}$ (pcm)	-1 ± 3	2 ± 3	0 ± 6
Abs. / Rel. Transport time (h/-)	4.9 / 0.95	2.6 / 0.97	7.3 / 0.98
$P_{\text{err,maj,DBRC}}$	8.2E-08	8.5E-08	5.4E-08

CAPTIONS FOR FIGURES

Figure 1 Majorant cross sections for different basis temperatures T_{base} (0 K and 300 K) and temperature differences (300 K, 600 K and 900 K) for the total cross section of ^{238}U around the 6.7 eV resonance.

Figure 2 The energy ranges are defined differently for the revised and the traditional majorant.

Figure 3 Effect of the conservativity of the TMS majorant on three k_{eff} estimators of a HTGR system. The effect is studied for the revised majorant and, thus, the conservativity is manipulated through the Q parameter. The error bars correspond to two standard deviations, 2 σ.

Figure 4 Effect of the conservativity of the TMS majorant on three different k_{eff} estimators of a HTGR system. The conservativity is manipulated through the h parameter of the traditional majorant.

Figure 5 Comparison of neutron flux spectra between two TMS calculations and NJOY-based reference solution. With Q=1E-4 (left) the flux spectrum corresponds to the reference, but with Q=3.2E-4 (right) significant differences can be recognized. The dashed line corresponds to two standard deviations.

Figure 8 Comparison of neutron flux spectra between two DBRC calculations and NJOY-based reference solution. With h=3.2E-3 (left) the flux spectrum corresponds to the reference, but with h=1.0E-2 (right) significant differences can be recognized.

CAPTIONS FOR TABLES

Table I Performance comparison between traditional and revised majorant when applying TMS method in three thermal systems.

Table II Performance comparison between traditional and revised majorant when applying DBRC method in three thermal systems.

Table III Final performance results for three test cases. The relative (rel.) values are calculated with respect to the "Reference" calculation, an ordinary Serpent calculation with DBRC and full optimization. The errors correspond to one sigma.

FOOTNOTES

a For a complete and up-to-date description, visit Serpent website — http://montecarlo.vtt.fi

b To be precise, also each cross section Σ_x for which $\Sigma_x(E) \geq \Sigma_{\mathrm{maj}}(E)$ can be considered a temperature majorant cross section of $\Sigma(E')$, but usually it is practical to choose the majorant according to Eq. (1).

c Also other ways of dealing with the energy dependence have been introduced: in Ref. [10] a technique based on direct sampling of the secondary neutron velocity has been examined, while in Refs. [11, 12] the correction is done by varying the particle weights. It is also possible to include the effect by using $S(\alpha, \beta)$ tables based on the analytical scattering kernel, which has been covered in sequential Refs. [13–15].

d The multiplication is required for correct modeling of the reaction rates at low energies and is related to the fact that the integral of the distribution from which the target velocities are sampled (Eq. (7)) is greater than unity at low energies. This modification is perhaps the most intuitive in case of potential scatterers with constant low-energy cross sections: these cross sections are increased in the Doppler-broadening process, but the corresponding increase in the reaction rates could not be captured in the TMS transport without multiplying the cross sections by g.

e Since this system is in practice a quasi-homogeneous mixture of moderator and fuel, the probability of a neutron to interact with the fuel material during the slowing-down process is very high compared to, for instance, LWR geometries. In addition, the fact that the moderator atoms in graphite are relatively heavy ($A_{\mathrm{C}} \approx 12$) increases the number of scattering events a neutron experiences during the process compared to lighter moderators like light water. This increases the probability of a neutron to end up at energies corresponding to resonances in the fuel material at some point of the slowing-down process and, thus, makes the interactions more probable on average.

f It was found in [17] that the variances and, consequently, also the Figures-of-Merit for all estimators including the flux estimator are significantly affected by the usage of the TMS method near strong resonances.